Multisubband electron transport in δ-doped semiconductor systems

Guo-Qiang Hai and Nelson Studart
Departamento de Física, Universidade Federal de São Carlos, 13565-905 São Carlos, São Paulo, Brazil

François M. Peeters
Department of Physics, University of Antwerp (UIA), B-2610 Antwerpen, Belgium
(Received 1 February 1995; revised manuscript received 11 May 1995)

The electron transport properties in δ-doped semiconductor systems are studied. The subband electronic structure of the δ-doped system is obtained by solving the coupled Schrödinger and Poisson equations. The screening of the quasi-two-dimensional electron gas is taken into account for the ionized impurity scattering through the matrix dielectric function within the random-phase approximation. The quantum and transport mobilities are calculated numerically as a function of the total electron density and the width of the doped layer at zero temperature. The intersubband scattering and the effect of empty subbands above the Fermi level on the electron mobilities are investigated. The calculated mobilities are in reasonable agreement with the available experimental results.

I. INTRODUCTION

In recent years, there has been increasing interest in the study of the electron transport properties in δ-doped semiconductor systems. The δ-doped systems are, in general, characterized by a rather high electron concentration, which makes them different from the other quasi-two-dimensional (Q2D) systems, such as heterojunctions and quantum wells. Typically, several subbands are occupied in a δ-doped system and the effects resulting from the occupation of several subbands are very important. An advantage of the actual system is that no interfaces are present to confine the electrons and ionized impurity scattering is by far the most important scattering mechanism.

A large number of experimental investigations[1–13] have been carried out on the electron transport properties in δ layers. However, the theoretical studies on the electron transport properties of δ-doped systems are limited in some way. Gillman *et al.*[2] reported the calculation results of temperature dependence of the average electron drift mobility in δ-doped GaAs and they found the same trends as found experimentally for the Hall mobility. But they did not give details about the calculation and the electron subband mobility at low temperature was not obtained. However, in δ-doped systems, the electrons in different subbands have very different mobilities. Gold *et al.*[14] studied theoretically the electron transport in structures with low doping concentration such that only the lowest subband is populated. They included the influence of the disorder in the doping layer on the density of states and screening effects. The mobility was calculated by using a multiple-scattering theory. Mezrin and Shik[15] calculated the electron mobility in heavily doped δ layers using screened Coulomb potential within the Thomas-Fermi approximation (TFA). Very recently, González, Krupski, and Szwacka[16] calculated the electron subband transport mobilities due to the ionized impurity scattering. The screening on the Coulomb scattering potential was taken into account within the random-phase approximation (RPA). In Refs. 15 and 16, the calculations for electron mobility were based on the electronic subband structure obtained within the semiclassical Thomas-Fermi approximation,[17,15] which yields analytical expressions for the effective confinement potential and subband wave functions. In doing so, they had assumed the impurity layer with zero thickness. Furthermore, the condition of a vanishing background acceptor concentration was used in Ref. 15. In order to introduce a finite background acceptor concentration, a variational approach was employed and the electron subband wave function and the transport mobilities were obtained up to three subbands in Ref. 16.

In this work, we study the electron subband mobilities in heavily doped δ layers. To describe the system more realistically in such a way that the results obtained can reflect the experimental situation, we calculate the electronic structure of the δ layer by solving self-consistently the coupled Schrödinger and Poisson equations. Although the calculation of the electron transport properties becomes more laborious using the numerical self-consistent results for the subband energies and wave functions, the distribution of the donors and acceptors and the exchange-correlation contribution of the 2D electron gas can be easily introduced. As a result, the influences of the doping concentration and the thickness of the doped layer on the electron subband mobility can be studied in contrast with previous works. In our calculation, the screening effects of the 2D electron gas on the scattering potential of the ionized impurity are included and the effect of the empty subbands above the Fermi level on the electron mobility is also investigated through the dielectric matrix within the RPA. The theory is applied to Si δ-doped GaAs structures.

The paper is organized as follows. The electronic structure of the system is presented in Sec. II. In Sec. III, the scattering potential and screening effects on it are described. The transport mobility obtained from the Boltzmann transport equations within the relaxation time approximation and the quantum mobility coming from the linear response theory are exhibited in Sec. IV. The numerical results for the electron mobilities and the comparison with experiments are discussed in Sec. V. We present our concluding remarks in Sec. VI.

II. ELECTRONIC STRUCTURE OF THE SYSTEM

We consider the following impurity distribution for a Si δ-doped GaAs structure,

$$n_D(z) = \begin{cases} N_D/W_D, & |z| < W_D/2 \\ 0, & |z| > W_D/2, \end{cases} \tag{1}$$

where N_D is the areal impurity concentration, W_D is the width of the doped layer, which is taken in the xy plane. For typical experimental conditions, we have $N_D \gtrsim 10^{12}/\text{cm}^2$ and $W_D \lesssim 100$ Å. At such a high doping level, the average distance between impurities is smaller than the effective Bohr radius $a_B = \hbar^2\epsilon_0/m^*e^2$ ($a_B \approx 100$ Å for GaAs) and the electron wave function of the individual Si donors overlaps strongly with each other. As a consequence, the donors no longer act as isolated trapping centers and an impurity band is formed just below the conduction band of GaAs. The electrons are free to move in the doping plane and they do not freeze out on the donors at low temperature. Due to the interaction between the ionized impurities and the delocalized electrons, an effective attractive potential is formed in the z direction, which confines the electrons close to the δ layer. The electron energy in this direction is quantized into discrete levels and a Q2D electron system is formed. In GaAs, a critical n-type doping concentration is about 0.3×10^{12} cm^{-2}.[13] In the low doping concentration regime below this critical Mott density, the electron wave functions of the individual donors do not have an important overlap with each other. No impurity band is formed and the conduction takes place by electrons that hop from one donor site to another. In this case, the electric conductivity vanishes at zero temperature. In the present work, we are interested in the electron transport in the δ-doped systems in the high doping concentration regime.

The conventional way to determine the electronic structure of the δ -doped system is to employ the so-called self-consistent calculation within the Hartree-Fock approximation.[18–20,11] It amounts to replace the exact many-particle potential by an average one. Each electron is assumed to move in a self-consistent potential $V_{\text{sc}}(z)$ and the coupled one-dimensional Poisson and Schrödinger equations have to be solved self-consistently. In such a calculation, the impurity distribution, the exchange-correlation potential of the 2D electron gas, and the nonparabolicity of the conduction band can be included. In another way, the electron subband energy and wave functions of the δ-doped system can be obtained within the semiclassical TFA. It has been proven that for a system with zero-thickness doping layer and vanishing background acceptor concentration, such an approximation yields the results that are equivalent to those obtained from the self-consistent approximation.[17] The advantage of the TFA is that it gives an analytical expression for the effective confinement potential and subband wave functions. However, it is difficult to take into account the thickness of the doped layer and the acceptor background.

In this work, the subband wave functions are obtained from a self-consistent solution of the one-dimensional Schrödinger and Poisson equations. The total electron energy and wave function can be written as

$$E_n(\vec{k}_\parallel) = E_n + \varepsilon(\vec{k}_\parallel) \tag{2}$$

and

$$\Psi_{n,\vec{k}_\parallel}(x,y,z) = \psi_n(z)\frac{1}{\sqrt{A}}\exp(i\vec{k}_\parallel \cdot \vec{r}_\parallel), \tag{3}$$

where n =1, 2,..., is the subband index, $\vec{r}_\parallel$ ($\vec{k}_\parallel$) is the electron position (wave vector) in the xy plane, E_n is the subband energy, $\psi_n(z)$ is the electron wave function in the z direction, $\varepsilon(\vec{k}_\parallel) = \hbar^2k_\parallel^2/2m^*$ is the electron kinetic energy, m^* the electron effective mass, and A is the area of the sample.

The Schrödinger equation in the z direction is given by

$$-\frac{\hbar^2}{2m^*}\frac{d^2\psi_n(z)}{dz^2} + V_{\text{sc}}(z)\psi_n(z) = E_n\psi_n(z), \tag{4}$$

where $V_{\text{sc}}(z) = V_H(z)+V_{\text{xc}}(z)$ is the effective confinement potential, which is composed as a sum of the Hartree potential $V_H(z)$ and exchange-correlation potential $V_{\text{xc}}(z)$. The Hartree potential, due to the electrostatic interaction of the electrons with themselves and with ionized impurities, is determined by the following Poisson equation:

$$\frac{d^2V_H}{dz^2} = \frac{4\pi e^2}{\epsilon_0}[n_e(z) - n_D(z) + n_A], \tag{5}$$

where $n_e(z)$ is the electron concentration distribution and n_A is the ionized background acceptor concentration. In Eq. (5), we assumed that all the donors in the doping layer are ionized. At zero temperature, the electron distribution is obtained by

$$n_e(z) = \sum_{n=1}^{N} |\psi_n(z)|^2 \int_{E_n}^{E_F} \rho(E)dE, \tag{6}$$

where N is the number of the occupied subbands, $\rho(E)$ is the electron density of states of the system, and E_F is the Fermi energy. For a parabolic conduction band, $\rho(E) = m^*/\pi\hbar^2$ is a constant for the 2D system. The effect of the nonparabolicity of the conduction band on the electronic subband structures can be included through

electron density of states (or the effective mass m^*). In the numerical calculations, we found that using the usual formalism for Q2D systems,[21] the nonparabolicity modifies the self-consistent solution slightly. So, we will not give the details here. The total electron density $N_e = \int_{-\infty}^{\infty} n_e(z)dz$ is determined by the difference between N_D and N_A, where N_A is the areal ionized acceptor concentration and can be estimated from the thickness of the depletion layer. For $n_A = 10^{14}/\text{cm}^3$, $N_A \simeq 10^{11}/\text{cm}^2$.

The exchange-correlation potential $V_{\text{xc}}(z)$ is a function of electron density and can be evaluated within the local-density approximation[22]

$$V_{\text{xc}}(z) = -\frac{e^2}{8\pi\epsilon_0 a_B}\frac{2}{\alpha\pi r_s}\left[1 + 0.0545\ln\left(1+\frac{11.4}{r_s}\right)\right], \tag{7}$$

where $\alpha = (4/9\pi)^{1/3}$ and $r_s = [4\pi n_e(z)/3]^{-1/3}/a_B$.

We performed a self-consistent calculation for the subband electronic structures of a Si δ-doped GaAs system.

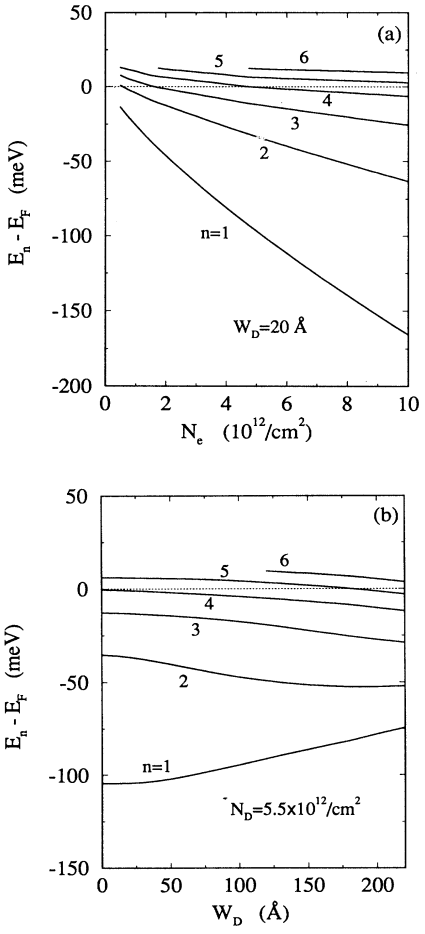

FIG. 1. The subband energy as a function of (a) total electron density for $W_D = 20$ Å and (b) the width of the doping layer for $N_D = 5.5 \times 10^{12}/\text{cm}^2$. The dotted line indicates the Fermi level.

In the calculation, we took the parameters $m^* = 0.07m_0$, $\epsilon_0 = 13.18$, and $n_A = 10^{14}/\text{cm}^3$. The electron exchange-correlation energy and the band nonparabolicity were included. We input the donor concentration N_D and the width of the doped layer W_D. The effective confining potential profile $V_{\text{sc}}(z)$, the subband energy E_n, the wave function $\psi_n(z)$, the Fermi energy E_F , and the subband electron population were obtained. We confirmed that the subband electron population density from our calculation is in good agreement with the electron densities obtained from Shubnikov–de Haas (SdH) experiments.[11,13]

Figure 1 shows the subband energy E_n as a function of (a) the total electron density N_e for $W_D = 20$ Å and (b) the thickness of the doped layer W_D for $N_D = 5.5 \times 10^{12}/\text{cm}^2$. In the figure, the energy level E_n is measured from the Fermi energy E_F, which is indicated by the dotted line. In Fig. 1(a) for $W_D = 20$ Å, only the lowest subband is populated at low electron density (low doping concentration). With increasing N_e (or N_D), the effective confinement potential becomes narrow and deep. The distance between two levels increases and more subbands are populated. The n=2, 3, and 4 subbands begin to be occupied at $N_e = 0.58$, 1.62, and $4.76\times10^{12}/\text{cm}^2$, respectively. With increasing W_D, we also find that more subbands are populated as shown in Fig. 1(b). In this case, however, the total electron density is fixed. Wide doped layers lead to a broad and shallow confinement potential.

III. SCATTERING POTENTIAL AND SCREENING

In the following, we will consider only the ionized donor scattering because it is the most important scattering mechanism for the considered system. The ionized impurities scattering potential is given by

$$V(\vec{r}) = -\sum_i \frac{e^2}{\epsilon_0}\frac{1}{|\vec{r}-\vec{R}_i|}, \tag{8}$$

where $\vec{R}_i$ is the position of the impurity, the sum runs over all the impurities in the system which are distributed randomly in the doped layer. The two-dimensional Fourier transform of the scattering potential is given by

$$v(q_\parallel, z) = -\frac{2\pi e^2}{\epsilon_0 q_\parallel}\sum_i e^{-q_\parallel|z-z_i|}e^{i\vec{q}_\parallel\cdot\vec{R}_{\parallel i}}, \tag{9}$$

where $\vec{R}_i = (\vec{R}_{\parallel i}, z_i)$.

In the calculation of the electron transport properties, we assume a parabolic conduction band. Using the Fermi golden rule, the electron transition probability from state $|n,\vec{k}_\parallel\rangle$ to $|n',\vec{k}'_\parallel\rangle$ for electron-impurity scattering is given by

$$W_{n,n'}(\vec{k}_\parallel,\vec{k}'_\parallel) = \frac{2\pi}{\hbar}|u_{n,n'}(\vec{q}_\parallel)|^2\delta_{\vec{k}'_\parallel-\vec{k}_\parallel,\vec{q}_\parallel} \times\delta[E_{n'}(k'_\parallel) - E_n(k_\parallel)], \tag{10}$$

where $u_{n,n'}(\vec{q}_\parallel)$ is the transition matrix element due to the scattering.

The present system has a rather high electron density and consequently the screening of the scattering potential due to the electron gas will be significant. The screened ionized impurity potential can be obtained in terms of the static dielectric response function within RPA. Because of the occupation of several subbands, the dielectric function has a tensor character given by $\epsilon_{\alpha,\beta}(\vec{q}_\parallel) = \epsilon_{nn',mm'}(\vec{q}_\parallel)$, where $\alpha = (n,n')$, $\beta = (m,m')$. If we assume that the impurities are uniformly distributed in the doped layer and are uncorrelated, the square of the transition matrix element due to the screened Coulomb scattering potential is given by

$$|u_{n,n'}(\vec{q}_\parallel)|^2 = \left(\frac{2\pi e^2}{\epsilon_0 q_\parallel}\right)^2 \frac{N_D}{W_D}\int_{-W_D/2}^{W_D/2} \times dz_i \left[\sum_\beta \epsilon^{-1}_{\alpha,\beta}(\vec{q}_\parallel) G_\beta(q_\parallel, z_i)\right]^2 \quad (11a)$$

and

$$G_\beta(q_\parallel, z_i) = \int_0^\infty dz \psi_m(z)\psi_{m'}(z)[e^{-q_\parallel|z-z_i|} + (-1)^{m+m'} e^{-q_\parallel|z+z_i|}], \quad (11b)$$

with the change in electron momentum due to scattering

$$q_\parallel = \left[(E_n - E_{n'})\frac{2m^*}{\hbar^2} + 2k_\parallel^2 - 2k_\parallel \cos\theta \sqrt{(E_n - E_{n'})\frac{2m^*}{\hbar^2} + k_\parallel^2}\right]^{1/2} \quad (11c)$$

and θ is the angle between $\vec{k}_\parallel$ and $\vec{k}'_\parallel$.

In the above equations, $\epsilon^{-1}_{\alpha,\beta}(\vec{q}_\parallel)$ is the element of the inverse matrix of the dielectric response function, and the sum $\beta = (m,m')$ runs over all the subbands of the system. In actual calculations, however, we have to limit the β sum. In most previous works, only the matrix elements of the dielectric function associated with the occupied subbands were considered. Consequently for a system of N occupied subbands, the dielectric function $\epsilon_{\alpha,\beta}(\vec{q}_\parallel)$ is approximated by a $N^2 \times N^2$ matrix. Following this approach, the subband mobilities in heterojunctions with two occupied subbands were studied in Refs. 23–25. And those in a δ-doped system with three occupied subbands were calculated in Ref. 16.

The dielectric function within the RPA is given by

$$\epsilon_{\alpha,\beta}(q_\parallel) = \delta_{\alpha,\beta} + \frac{2}{a_B q_\parallel} F_{\alpha,\beta}(q_\parallel)\chi^0_\beta(q_\parallel), \quad (12a)$$

where

$$F_{\alpha,\beta}(q_\parallel) = \int_{-\infty}^\infty dz \psi_n(z)\psi_{n'}(z) \times \int_{-\infty}^\infty dz' \psi_m(z')\psi_{m'}(z') e^{-q_\parallel|z-z'|} \quad (12b)$$

is the Coulomb form factor and $\chi^0_\beta(\vec{q}_\parallel)$ is the static electron density-density correlation function[23,24,26–28] without the electron-electron interaction. Notice that $\chi^0_{mm'}(\vec{q}_\parallel) = 0$ only when both the subbands m and m' are empty, and $\chi^0_{mm'}(\vec{q}_\parallel) \neq 0$ as long as one of the them is populated. It means that the unoccupied subbands have contributions to the intersubband interaction of the Q2D electron gases.[28] They could also influence the intrasubband interaction of the occupied subbands through the mode coupling between the intrasubband and intersubband excitations. Such an effect in the collective excitations of the Q1D electron system with a three-band model (one of them was empty), was investigated in Ref. 30.

IV. TRANSPORT EQUATIONS

Considering only the ionized impurity scattering, we calculate the electron subband quantum and transport mobilities. These are determined from the different scattering times connected to the average time between the scattering events. The quantum lifetime or the single particle relaxation time is the averaged elastic scattering time. On the other hand, in the transport lifetime or the momentum relaxation time, every scattering event is averaged over its projection of the outgoing wave vector on the incident direction.[13] The Boltzmann equation of the δ-doped system for steady-state transport can be written as

$$-\frac{e}{m^*}\hbar\vec{k}_\parallel \cdot \vec{E}_\parallel \frac{\partial f_n(\vec{k}_\parallel)}{\partial \varepsilon(\vec{k}_\parallel)} = \sum_{n',\vec{k}'_\parallel} W_{n,n'}(\vec{k}_\parallel, \vec{k}'_\parallel) \times [f_{n'}(\vec{k}'_\parallel) - f_n(\vec{k}_\parallel)], \quad (13)$$

where $W_{n,n'}(\vec{k}_\parallel, \vec{k}'_\parallel)$ is given by Eq. (10), and $f_n(\vec{k}_\parallel)$ is the electron distribution function. Notice that $W_{n',n}(\vec{k}'_\parallel, \vec{k}_\parallel) = W_{n,n'}(\vec{k}_\parallel, \vec{k}'_\parallel)$.

Within the relaxation time approximation, the distribution function can be written as[29,19]

$$f_n(\vec{k}_\parallel) = f_n^{(0)}(\vec{k}_\parallel) + \frac{e}{m^*}\hbar\vec{k}_\parallel \cdot \vec{E}_\parallel \frac{\partial f_n^{(0)}(\vec{k}_\parallel)}{\partial \varepsilon(\vec{k}_\parallel)} \tau_n^t(\varepsilon),$$

where $f_n^{(0)}$ is the Fermi-Dirac distribution function and $\tau_n^t(\varepsilon)$ is the so-called subband transport lifetime (momentum relaxation time). The Boltzmann equation can be reduced to a coupled linear equation about $\tau_n^t(\varepsilon)$.[29] At $T = 0$, only the electrons on the Fermi surface contribute to electric transport and we have $\tau_n^t = \tau_n^t(E_{Fn})$, where $E_{Fn} = E_F - E_n$. For a system of N subbands populated, the electron subband transport lifetime is determined by the equations

$$\sum_{n'=1}^N K_{n,n'}\tau_n^t = 1 \quad \text{for } n = 1, 2, ..., N \quad (14a)$$

with

$$K_{n,n} = \frac{m^*}{\pi\hbar^3}\left\{\int_0^\pi d\theta |u_{n,n}(q'_\parallel)|^2(1-\cos\theta) + \sum_{n'\neq n}^{N}\int_0^\pi d\theta |u_{n,n'}(q'_\parallel)|^2\right\}, \quad (14b)$$

and, for $n' \neq n$,

$$K_{n,n'} = \frac{m^*}{\pi\hbar^3}\sqrt{\frac{E_{Fn'}}{E_{Fn}}}\int_0^\pi d\theta |u_{n,n'}(q'_\parallel)|^2\cos\theta, \quad (14c)$$

where

$$q'_\parallel = \frac{2m^*}{\hbar^2}\left[E_{Fn} + E_{Fn'} - 2\sqrt{E_{Fn}E_{Fn'}}\cos\theta\right]^{1/2}. \quad (14d)$$

The quantum mobility or the single-particle mobility τ_n^q is determined by the average scattering time. Within the linear response theory, the subband quantum lifetime is given by[24]

$$\frac{1}{\tau_n^q} = \frac{m^*}{\pi\hbar^3}\sum_{n'=1}^{N}\int_0^\pi d\theta |u_{n,n'}(q'_\parallel)|^2. \quad (15)$$

From the transport and quantum lifetime, the electron subband transport mobility and quantum mobility can be obtained easily,

$$\mu_n^t = \frac{e}{m^*}\tau_n^t, \qquad \mu_n^q = \frac{e}{m^*}\tau_n^q. \quad (16)$$

Notice that the empty subbands $n > N$ do not appear in the transport equations (14) and (15) which determine the electron mobilities. They are not involved in the scattering processes directly. However, the empty subbands influence the impurity scattering potential through screening effects, which is taken into account by the dielectric function.

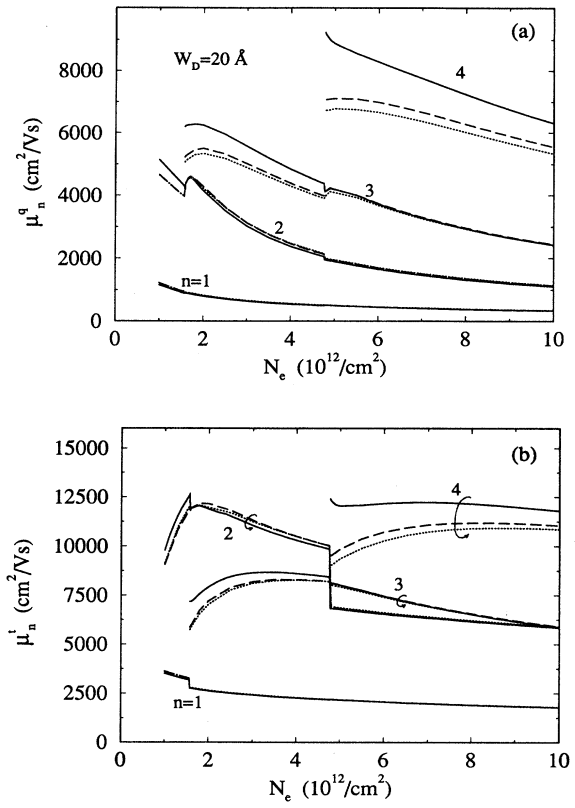

FIG. 2. The subband (a) quantum mobility and (b) transport mobility as a function of the total electron density for $W_D = 20$ Å. The solid, dashed, and dotted curves present the results including 0, 1, and 2 empty subbands in the dielectric matrix, respectively.

V. NUMERICAL RESULTS AND DISCUSSION

Using the previous results for the transport properties, we calculated the electron transport mobility and the quantum mobility in the δ layer. In Fig. 2, the electron subband (a) quantum mobility and (b) transport mobility for the Si δ-doped GaAs structures of $W_D = 20$ Å are plotted as a function of the total electron density. The solid curves indicate the results considering only the N occupied subbands in the dielectric function, which is approximated by a $N^2 \times N^2$ matrix. The dashed and dotted curves present the results including one and two empty subbands, respectively, in the dielectric function, which is given by a $(N+1)^2 \times (N+1)^2$ and a $(N+2)^2 \times (N+2)^2$ matrix. It is seen that the empty subbands above the Fermi level indeed influence the electron mobility through the effect of the screening on the Coulomb scattering in the present multisubband system. Such an influence on the mobility of the electrons in the higher subband is stronger than in the lower ones. Both the quantum and transport mobilities coming from the highest occupied subband are depressed due to the effects related to the empty subbands. However, such an influence on the mobilities from the lower subbands is not pronounced.

We found that the quantum mobility, as shown in Fig 2(a), increases with increasing subband index and decreases with increasing total electron density (or donor concentration). At the onset of occupation of a new subband, the theoretical subband mobility exhibits an abrupt jump. Such a discontinuity is due to the intersubband scattering and has been discussed in Refs. 16, 23, and 24 for the multisubband transport in Q2D systems. However, for the transport mobility, as shown in Fig. 2(b), $\mu_2^t > \mu_3^t$ when only three subbands are populated, which is qualitatively in agreement with the results in Ref. 16. This is mainly due to the fact that the wave function $\psi_2(z)$ is antisymmetric and has a node at $z = 0$. For a narrow doped layer, electrons in this subband have a smaller overlap with the impurities than those in the third subband and, consequently, the scattering is weaker. After the onset of occupation of the $n = 4$ subband, μ_2^t becomes smaller than μ_3^t. This is because $\psi_2(z)$ and $\psi_4(z)$ have the same parity, and the intersubband

scattering between them is strong. We also observe that the transport mobilities due to the $n = 2$ and $n = 3$ subbands are close to each other and much higher than those of the lowest subband. When we compare the present results of the transport mobilities obtained by considering only the occupied subbands in the screening [solid curves in Fig. 2(b)] with those of Ref. 16, we observe that the Fig. 4 in Ref. 16 shows (i) at the onset of the occupation of the third subband, the transport mobility of the lowest subband decreases abruptly by about a factor of 4, while the mobility of the second subband has an increasing jump; (ii) when three subbands are occupied, the mobility of the lowest subband increases with increasing the doping concentration (electron density); and (iii) the mobility of the second subband is about a factor of 6 larger than that of the third subband. In contrast, our calculation shows that at the onset of the occupation of the third subband, the mobility of the two lower subband decrease about 6% and 15%, respectively. The mobility of the lowest subband decreases with increasing the doping concentration, and the mobilities of the second and the third subband are close to each other, which are in agreement with experimental results.[5–7,9,11]

Figure 3 shows the electron transport mobility as a function of the width of the doping layer for fixed doping concentration (a) $N_D = 2 \times 10^{12}/\text{cm}^2$ and (b) $N_D = 8 \times 10^{12}/\text{cm}^2$. The mobilities corresponding to n =1, 2, 3, and 4 subbands are indicated by solid, dashed, dotted, and dotted-dash curves, respectively. In Fig. 3 and hereafter, the mobilities are obtained by including all the occupied subbands and two empty subbands above E_F in the dielectric matrix. It is seen that by increasing the width of the doping layer, the mobility of electrons in the lowest subband μ_1^t increases slowly, while those corresponding to higher subbands have a stronger width dependence than in the case of occupation of the lowest subband. For narrow layers, the higher subbands show a much larger mobility than the lowest one, which is a consequence of the fact that the electrons in the higher subbands are mainly situated away from the $z = 0$ plane. By increasing W_D, μ_2^t and μ_4^t decrease rapidly and μ_2^t becomes very close to μ_1^t for wider layers. μ_3^t increases slowly till a maximum is reached at $W_D \simeq 100$ Å for $N_D = 2 \times 10^{12}/\text{cm}^2$ [Fig. 3(a)] and at $W_D \simeq 50$ Å for $N_D = 8 \times 10^{12}/\text{cm}^2$ [Fig. 3(b)] and then decreases. The position of this maximum shifts to smaller W_D as one increases the doping concentration. The abrupt decrease of the mobility at $W_D = 105$ Å in Fig. 3(b) is due to the onset of the occupation of the $n = 5$ subband. For small W_D, μ_2^t and μ_3^t are close to each other. In Fig. 3(a), $\mu_2^t > \mu_3^t$ when $W_D < 65$ Å because the overlap of $|\psi_3(z)|^2$ with the doped layer is stronger than that of $|\psi_2(z)|^2$ in this case. However, by increasing W_D, such an overlap increases much faster for the $n = 2$ than for $n = 3$ subband. Notice that with increasing W_D, the transport mobilities of the subbands with antisymmetric wave function (n =2, 4) decrease monotonously. However, for those subbands with symmetric wave function (n =1, 3), μ_1^t increases monotonously and a maximum mobility in μ_3^t appears.

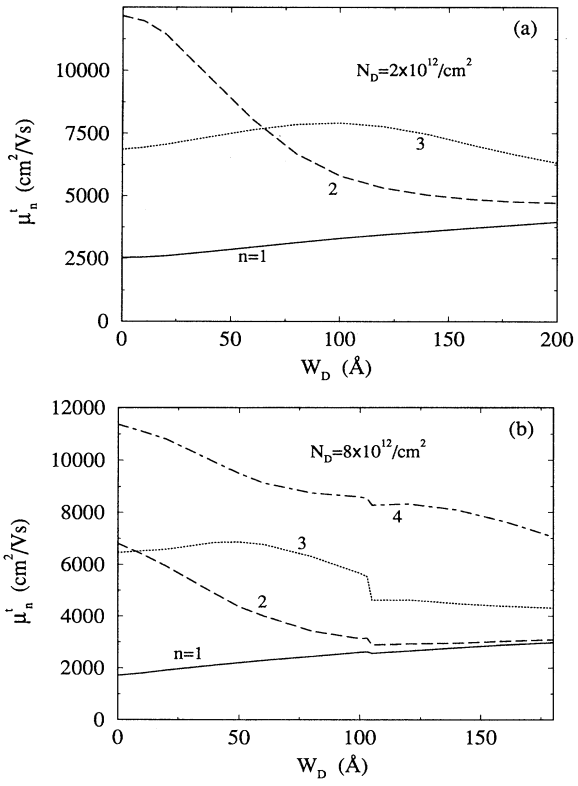

FIG. 3. The transport mobility as a function of the width of the doped layer for (a) $N_D = 2 \times 10^{12}/\text{cm}^2$ and (b) $N_D = 8 \times 10^{12}/\text{cm}^2$. The solid, dashed, dotted, and dotted-dashed curves present the results of the subbands n =1, 2, 3, and 4, respectively.

In Fig. 4, the electron quantum mobility is plotted as a function of the width of the doped layer for (a) $N_D = 2 \times 10^{12}/\text{cm}^2$ and (b) $8 \times 10^{12}/\text{cm}^2$. We found that the W_D dependence of the quantum mobility has a similar behavior as the transport mobility. However, at small W_D, the quantum mobilities due to the different subbands are well separated and increase with the order of the subband index. By increasing W_D, μ_1^q increases slowly and μ_2^q decreases and they approach each other at large W_D. In Fig. 4(b), $\mu_1^q \simeq \mu_2^q$ for $W_D > 100$ Å. In contrast to transport mobility, μ_3^q is much larger than μ_2^q in the whole calculated range of W_D.

We have compared our calculation with available experimental results of subband transport and quantum mobilities.[11,13,4,7,5] Experimentally, the quantum mobility is obtained by the SdH measurements[4,13] and the transport mobility is obtained by the so-called mobility spectrum technique[31,6,13] or by the Hall measurements combining with the subband electron density from the SdH measurements.[1,4] The experimental results used here were obtained at liquid helium temperature (4.2 K) or lower. The uncertainties of the quantum mobilities of the lowest two subbands are about 10%. For the higher subbands with subband electron density less than 3×10^{11} cm^{-2}, the relative error of the experimental results is much larger. The electron density dependence of the transport and quantum mobilities is shown in Figs.

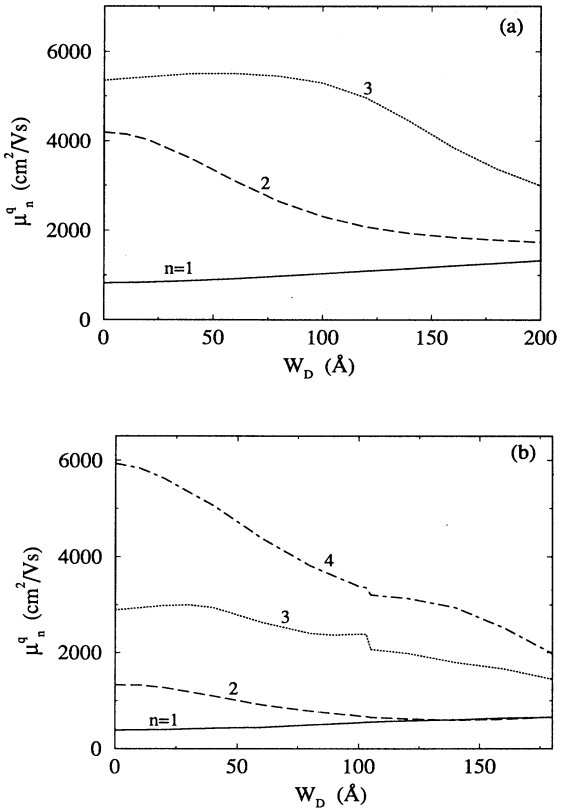

FIG. 4. The same as Fig. 3 but now for the quantum mobility.

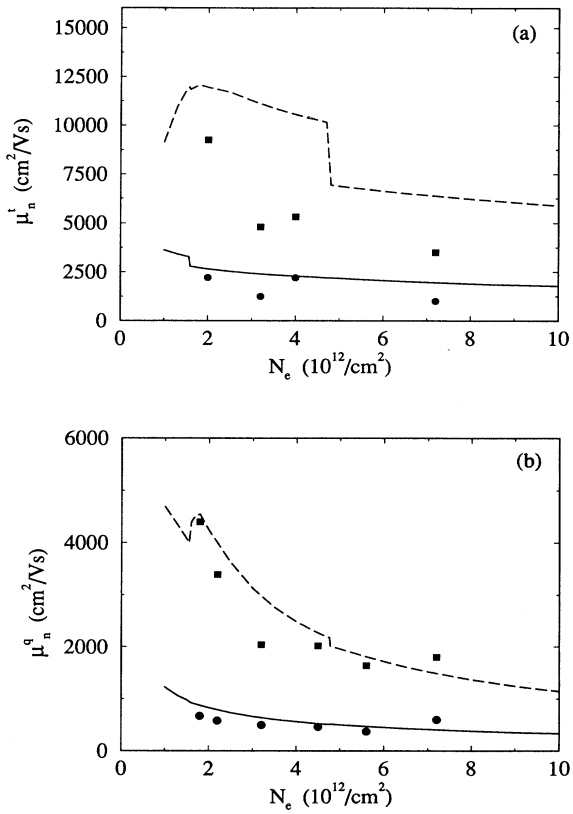

FIG. 5. The electron density dependence of (a) the transport mobility and (b) the quantum mobility in Si δ-doped GaAs. The solid and dashed curves present the calculated mobilities of the n =1 and 2 subbands, respectively, for W_D = 20 Å. The experimental results are indicated by the solid circles (n = 1) and squares (n = 2). The experimental results are from Refs. 5 and 11, but the results at $N_e = 7.2 \times 10^{12}/\text{cm}^2$ are from Ref. 4 and the results of transport mobilities at $N_e = 4.0 \times 10^{12}/\text{cm}^2$ are from Ref. 7.

5(a) and 5(b), respectively. In this figure, the calculated mobilities of the first two subbands for W_D = 20 Å are given by the solid (n = 1) and dashed (n = 2) curves. The experimental results of a Si δ-doped GaAs are indicated by solid circles (n = 1) and squares (n = 2). For the transport mobility in Fig. 5(a), our calculation shows the correct qualitative behavior as found experimentally. Quantitatively, the calculated transport mobility of n = 1 subband has a better agreement with experimental measurements than that of n = 2 subband, which is about a factor of 2 larger than observed experimentally for $N_e > 3.0 \times 10^{12}/\text{cm}^2$. At the onset of the population of a new subband, the theoretical subband mobility exhibits an abrupt decrease, which is not seen experimentally. This is probably due to the fact that in real systems there exist thickness fluctuations in the doped layer, which lead to fluctuations in E_n. However, in Fig. 5(b), the calculated quantum mobility shows a quite good agreement with the experimental results.

In Fig. 6, the quantum mobility is given as a function of the width of doped layer W_D for Si δ-doped GaAs of $N_D = 5.5 \times 10^{12}/\text{cm}^2$. The theoretical (experimental) quantum mobilities are presented by solid curve (circles) for n = 1, dashed curve (squares) for n = 2, and dotted curve (triangles) for n = 3. We found that for the first two subbands, the calculated mobility is in good agreement with the experimental results. By increasing W_D, μ^q_1 increases slowly and μ^q_2 tends to μ^q_1 at $W_D > 120$

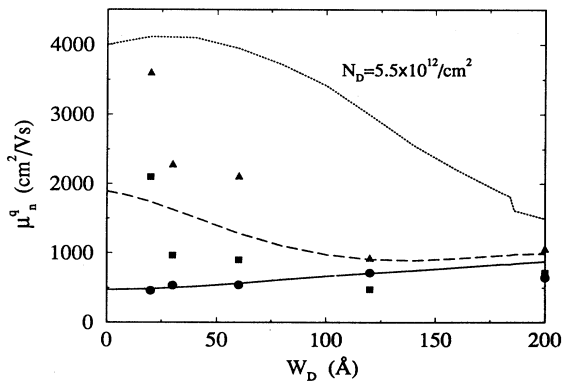

FIG. 6. The dependence of quantum mobility on the width of the layer for Si δ-doped GaAs with $N_D = 5.5 \times 10^{12}/\text{cm}^2$. The solid, dashed, and dotted curves present the calculated results of the n =1, 2 and 3, respectively. The experimental results are indicated by the solid circles (n = 1), squares (n = 2), and triangles (n = 3) (Refs. 11 and 13).

Å. For the higher subband n =3, the calculated mobility shows qualitatively similar W_D dependence as found experimentally.

We also found that the ratio of the transport mobility to the quantum mobility from our calculation increases with increasing the doping concentration. But it is almost not influenced by the thickness of the doped layer. In the range of the doping concentration considered, it increases from three to six for the lowest two subbands and from one to three for the third one. Experimentally, this ratio was found to be in the range $1.3 - 2.9$ for the δ-layer structure[11,13] and it is about two for the δ-doped quantum wells.[9] The ratio of the transport to the quantum mobility reflects the nature of the scattering mechanism, i.e., long-range versus short-range scattering. It is seen that the present calculation yields a higher transport mobility than the experimental result. It seems that the model of the screened Coulomb scattering potential with static RPA describes the short-range scattering more exactly than the long-range scattering.

In the present calculation, only the scattering of ionized donors is considered. Even though ionized impurity scattering dominates the electron mobility in δ-doped systems, there are several unknown factors, which can modify the electron transport properties. For instance, from an experimental point of view, the profile of the impurity layer and the effective thickness of the doping layer are not always exactly known. In heavily doped semiconductor systems, the random distribution of the impurities induces a band tail and creates localized states. Then the density of states of the δ-doped system is no longer a steplike function. Because of the localized states and the deep level centers, the electron density becomes much lower than the intended doping concentration at high doping level. For the present system, this is expected to be relevant for $N_D > 6 \times 10^{12}$ cm^{-2}. Other scattering mechanisms will also influence the electron mobility slightly, such as scattering with ionized acceptors, neutral impurities, and the electron-electron interaction. Deep level centers and the presence of possible impurity clusters may also play a role. Because of the high impurity concentration, the correlation among the impurities becomes important and should be considered. Besides, the screening is an important factor that influences the electron-impurity scattering. In the theoretical study of the electron transport properties in Q2D systems, the static RPA screening is often used. In principle, all the energy states in the system, including the screening effects, and the full energy spectrum should be considered in the dielectric function within RPA for a multisubband system. In the present calculation, we included all the occupied subbands and two empty subbands above E_F in the dielectric function. In such a case, the numerical calculation was already very difficult for four or five populated subbands.

In our calculation, we assumed a steplike electron density of states for each subband of the Q2D systems. This is justified when the subbands are well separated in energy and are much larger than the band tail of localization states. This is the case for the first few subbands. When there is a band tail at the onset of subband occupation, the Fermi level will cross the mobility edge of the subband leading to a different scattering rate.

VI. CONCLUSIONS

In summary, the electron transport properties in δ-doped semiconductor systems have been studied. Our mobility calculations were based on the self-consistent solution of the subband electronic structure and wave functions. The influences of the doping concentration and the thickness of the doped layer on the electron subband transport and quantum mobilities were investigated. The ionized donor scattering was considered and the screening was included within the static RPA for the multisubband 2D system. To the best of our knowledge, this is the first work where the self-consistent electronic structure of δ-layers has been used to investigate the subband quantum and transport mobilities. The effects due to the thickness of the doped layer on the subband mobility and due to use of empty subbands in the screening of 2D electron gas were also studied.

Our calculation shows that the electrons in the lowest subband have a low mobility, which is not much influenced by the doping concentration and the thickness of the doped layer. The mobilities due to the occupation of higher subbands are much bigger than those of the lowest one for small W_D, and they are strongly dependent on the different parameters. We demonstrated that intersubband scattering is also important, as we have seen at the onset of the occupation of a new subband. Although the empty subbands are not involved in the solution of the Boltzmann transport equation at zero temperature, they affect the electron mobility through screening effects on the scattering potential. The result of our calculation shows that the empty subbands modify the subband mobility, especially for the highest occupied subband. So, in this way our calculation includes the important effect of the mode coupling between the intrasubband and intersubband excitations that has been shown to be relevant in multisubband models of plasmon excitations. We also observed that is very important to obtain an accurate electronic structure for the mobility calculations. For instance, the position of the onset of the population of a new subband determines where a new scattering channel is introduced, which leads to the discontinuity in mobility.

Our calculated quantum mobilities of the lowest two subbands, both for N_e dependence and W_D dependence, are in quite good agreement with experimental results from Shubnikov–de Haas measurements.[11,13] The transport mobilities and the quantum mobilities of higher subbands have the same behavior as observed experimentally but, quantitatively, they are larger than experimental results.

ACKNOWLEDGMENTS

One of us (G.Q.H.) wishes to thank Conselho Nacional de Desenvolvimento Científico e Tecnológico (CNPq), Brazil, for financial support. F. M. P acknowledges financial support by the Belgian National Science Foundation.

[1] A. Zrenner, F. Koch, J. Leotin, M. Goiran, and K. Ploog, Semicond. Sci. Technol. **3**, 1132 (1988).
[2] G. Gillman, B. Vinter, E. Barbier, and A. Tardella, Appl. Phys. Lett. **52**, 972 (1988).
[3] E. F. Schubert, J. E. Cunningham, and W. T. Tsang, Solid State Commun. **63**, 591 (1987).
[4] E. Skuras, R. Kumar, R. L. Williams, R. A. Stradling, J. E. Dmochowski, E. A. Johnson, A. Mackinnon, J. J. Harris, R. B. Beall, C. Skierbeszewski, J. Singleton, P. J. van der Wel, and P. Wisnieski, Semicond. Sci. Technol. **6**, 535 (1991).
[5] P. M. Koenraad, F. A. P. Blom, C. J. G. M. Langerak, M. R. Leys, J. A. A. J. Perenboom, J. Singleton, S. J. R. M. Spermon, W. C. van der Vleuten, A. P. J. Voncken, and J. H. Wolter, Semicond. Sci. Technol. **5**, 861 (1990).
[6] P. M. Koenraad, B. F. A. van Hest, F. A. P. Blom, R. van Dalen, M. Leys, J. A. A. J. Perenboom, and J. H. Wolter, Physica B **177**, 485 (1992).
[7] G. M. Gusev, Z. D. Kvon, D. I. Lubyshev, V. P. Migal, and A. G. Pogosov, Fiz. Tekh. Poluprovodn. **25**, 601 (1991) [Sov. Phys. Semicond. **25**, 364 (1991)].
[8] I. A. Panaev, S. A. Studenikin, D. I. Lubyshev, and V. A. Migal, Semicond. Sci. Technol. **8**, 1822 (1993).
[9] J. J. Harris, R. Murray, and C. T. Foxon, Semicond. Sci. Technol. **8**, 31 (1993).
[10] X. Zheng, T. K. Carns, K. L. Wang, and B. Wu, Appl. Phys. Lett. **62**, 504 (1993).
[11] P. M. Koenraad, A. C. L. Heessels, F. A. P. Blom, J. A. A. J. Perenboom, and J. H. Wolter, Physica B **184**, 221 (1993).
[12] P. Sobkowicz, Z. Wilamowski, and J. Kossut, Semicond. Sci. Technol. **7**, 1155 (1992).
[13] P. M. Koenraad, in *Delta Doping of Semiconductors*, edited by E. F. Schubert (Cambridge University Press, Cambridge, 1995).
[14] A. Gold, A. Ghazali, and J. Serre, Semicond. Sci. Technol. **7**, 972 (1992).
[15] O. Mezrin and A. Shik, Superlatt. Microstruct. **10**, 107 (1991).
[16] L. R. González, J. Krupski, and T. Szwacka, Phys. Rev. B **49**, 11 111 (1994).
[17] L. Ioriatti, Phys. Rev. B **41**, 8340 (1990).
[18] A. Zrenner, F. Koch, and K. Ploog, Surf. Sci. **196**, 671 (1988).
[19] G. Bastard, *Wave Mechanics Applied to Semiconductor Heterostructures* (Halsted Press, New York, 1988), p. 193.
[20] M. H. Degani, Phys. Rev. B **44**, 5580 (1991).
[21] U. Ekenberg, Phys. Rev. B **36**, 6152 (1987); **40**, 7714 (1989).
[22] L. Hedin and B. I. Lundqvist, J. Phys. C **4**, 2064 (1971).
[23] S. Mori and T. Ando, Phys. Rev. B **19**, 6433 (1979).
[24] R. Fletcher, E. Zaremba, M. D'Iorio, C. T. Foxon, and J. J. Harris, Phys. Rev. B **41**, 10 649 (1990).
[25] W. Xu, F. M. Peeters, and J. T. Devreese, Phys. Rev. B **48**, 1562 (1993).
[26] F. Stern, Phys. Rev. Lett. **18**, 542 (1967).
[27] J. K. Jain and S. Das Sarma, Phys. Rev. B **36**, 5949 (1987).
[28] W. H. Backes, F. M. Peeters, F. Brosens, and J. T. Devreese, Phys. Rev. B **45**, 8437 (1992).
[29] E. D. Siggia and P. C. Kwok, Phys. Rev. B **2**, 1024 (1970).
[30] Q. Li and S. Das Sarma, Phys. Rev. B **40**, 5860 (1989); **43**, 11 768 (1991).
[31] W. A. Beck and J. R. Anderson, J. Appl. Phys. **62**, 541 (1992).